Journal of ELECTRONIC MATERIALS, Vol. 40, No. 12, 2011
DOI: 10.1007/s11664-011-1771-1

Metal-Assisted Chemical Etching Using Tollen's Reagent to Deposit Silver Nanoparticle Catalysts for Fabrication of Quasi-ordered Silicon Micro/Nanostructures

XUEWEN GENG,[1,2,5] MEICHENG LI,[3] LIANCHENG ZHAO,[1] and PAUL W. BOHN[2,4,6]

1.—School of Materials Science and Engineering, Harbin Institute of Technology, No.92, West Da-Zhi Street, Harbin 150001, Heilongjiang, People's Republic of China. 2.—Department of Chemical and Biomolecular Engineering, University of Notre Dame, Notre Dame, IN 46556, USA. 3.—Renewable Energy School, North China Electric Power University, Beijing 102206, People's Republic of China. 4.—Department of Chemistry and Biochemistry, University of Notre Dame, Notre Dame, IN 46556, USA. 5.—e-mail: gengxuewen@gmail.com. 6.—e-mail: pbohn@nd.edu

Metal-assisted chemical etching (MacEtch) of semiconductor materials in HF/H_2O_2 solution using noble-metal particles as catalysts has gained much attention in the past few years due to its unique properties. In this work, nanoscale Ag particles were deposited on (100) and (111) surfaces of polished *p*-Si wafers through the silver-mirror reaction. Subsequently these wafers were etched in 1:1:1 (v:v:v) HF(49%):H_2O_2(30%):EtOH solution at ambient temperature and pressure for 12 h, producing a number of different quasi-ordered silicon micro/nanostructures. The resulting surface-modified wafers exhibited mixed micro- and nanostructures that are an inherent feature of the etch process; for example, steps appear on the sidewalls of crystallographically defined nanopores, because the catalytic Ag nanoparticles are convected as they transit the developing pore during the etching process. The resulting materials exhibited much reduced reflectivity, reaching a maximum of 3.7× reduction near 330 nm, which renders them of interest in potential applications such as back-reflector templates for deposition of thin-film solar cell materials.

Key words: Metal-assisted chemical etching, porous silicon, nanopore, antireflection

INTRODUCTION

The rapid development of miniaturized structures demands smaller, faster, smarter, and more functional materials that, in turn, challenge semiconductor processing technologies to keep pace, especially techniques for manipulating silicon in three dimensions on micrometer and nanometer length scales. Especially challenging is the development of subwavelength structures for optoelectronic applications. The mechanical V-texture method,[1] laser processing,[2] electron-beam lithography and fast-atom beam etching,[3] reactive-ion etching (RIE),[4] and electron cyclotron resonance plasma etching[5] need sophisticated and expensive equipment, while newer techniques such as self-masking damage-free RIE are promising[6] but are not yet ready for large-scale use.

The recently developed metal-assisted chemical etching (MacEtch) method[7–10] has potential as a simple approach to fashion materials at nanometer length scales, while being compatible with common industrial processes. MacEtch is suitable for variously doped single- and polycrystalline bulk silicon[11] as well as thin silicon film[12] and even GaN.[10,13] It has been successfully used to fabricate high-sensitivity hydrogen sensors,[13] antireflective layers in efficient solar cells,[14] large-scale $Si_{1-x}Ge_x$ quantum dots,[15] silicon nanowire *p–n* junction diode

(Received June 22, 2011; accepted September 13, 2011; published online September 29, 2011)

arrays,[16] light-emitting silicon nanowire arrays,[17] and controlled complex three-dimensional (3D) templates.[18,19]

Various noble-metal particle catalysts have been successfully used to mediate the MacEtch process, however Ag particles are most commonly chosen to etch *p*-Si.[20–25] The final etched morphologies vary depending on the detailed etching conditions, including the method of Ag deposition, crystal orientation and doping, etch solution composition, etc.; for example, etching of Ag particles deposited by thermal evaporation or sputtering on *p*-Si (111) and *n*-Si (110) produces obliquely oriented, highly aligned Si nanowire arrays[21] and ordered, vertically aligned [110] nanowire arrays, respectively.[23] However, etching of *p*-Si (111) using Ag nanoparticles produced by electroless displacement from aqueous Ag^+/HF results in vertical Si nanowires.[26] Furthermore, Si etching can be altered from anisotropic to isotropic by varying the molar ratio of H_2O_2 and HF.

Mechanisms proposed to explain Si MacEtch in HF/H_2O_2[20,24] can be divided into two classes, differing principally according to the method of Ag deposition. The mechanism proposed[9] for dry deposition methods is as follows:[17–19,23]

Cathode reaction (at Ag)

$$H_2O_2 + 2H^+ \rightarrow 2H_2O + 2h^+ \quad (1)$$

$$2H^+ + 2e^- \rightarrow H_2\uparrow \quad (2)$$

Anode reaction (at Si)

$$Si + 4h^+ + 4HF \rightarrow SiF_4 + 4H^+ \quad (3)$$

$$SiF_4 + 2HF \rightarrow H_2SiF_6 \quad (4)$$

Overall reaction

$$Si + H_2O_2 + 6HF \rightarrow 2H_2O + H_2SiF_6 + H_2\uparrow \quad (5)$$

The other proposed mechanism invokes the working principle of a galvanic cell,[16,23,25–28] in which wet deposition of Ag particles is induced by Si-mediated reduction of Ag^+ in the presence of F^- as[27]

$$Si_{(s)} + 6F^-_{(aq)} + 4Ag^+_{(aq)} \rightarrow 4Ag_{(s)} + SiF^{2-}_{6(aq)} \quad (6)$$

In this case, the original Ag nucleation sites are random, but the localized areas beneath the particles etch first and serve as activated pits for pore growth, accompanied by translocation of particles into the growing pores, leading to formation of either a porous layer[25] or nanowire arrays.[23]

The work described herein uses the simple silver-mirror reaction utilizing Tollen's reagent[29] to deposit Ag particles on polished *p*-Si (100) and (111) surfaces, thereby avoiding Si-mediated redox processes. When metal-coated substrates prepared by this approach are subjected to MacEtch in HF/H_2O_2 solutions, unique morphologies are observed, exhibiting unusual micro/nanostructures, varying as a function of crystal face and etch conditions. The observed behavior suggests an etching mechanism similar to that given in Eqs. (1)–(5), and the combination of nanoscale and microscale roughness features supports potential applications in solar cell fabrication.

RESULTS AND DISCUSSION

Silver Deposition

The silver-mirror reaction produces granular Ag particles on *p*-Si (100) and *p*-Si (111) substrates, as shown in Fig. 1. The scanning electron microscopy (SEM) results are augmented by x-ray photoelectron spectroscopy (XPS) analysis, which is shown for Ag-decorated *p*-Si (100) in Fig. 2. The XPS spectrum of *p*-Si (111) (not shown) produces similar results. The Ag particles are distributed uniformly and at high density on both substrates, consistent with the observation of strong Ag peaks in the XPS spectrum. The particles are aggregated in the size range from 100 nm to 1 μm, with most aggregates ≥500 nm (Electronic Supplementary Material, Fig. S2). Since most of the particles in the thick Ag films aggregated into clusters, detailed particle size analysis was precluded. Although silver-mirror reactions were carried out under the same experimental conditions for both crystal orientations, the shapes of Ag particles exhibit subtle differences when deposited on (100) and (111) wafers; for example, although hexagonal-aspect particles, such as the particle highlighted in Fig. 1d, are found on both surfaces, they are far more prevalent on Si (111). The detailed reason for these differences are still being studied, but the observation is similar to the deposits of metals on mica,[30] where nanometer-scale, face-centered-cubic metals tend to nucleate and grow into twinned and multiply twinned particles with their surfaces bounded by the lowest-energy (111) facets. Similar hexagonal plates with the flat and bottom faces bounded by ⟨111⟩ plane were also observed in the controllable growth of Ag nanostructures on *p*-Si (111) wafers by a simple replacement reaction.[31]

Ag-Catalyzed MacEtch of Silicon

Ag-catalyzed MacEtch of *p*-Si of either orientation in $HF:H_2O_2$:ethanol (EtOH) is accompanied by evolution of bubbles throughout the 12 h etch. Even though deep pores are not observed when micrometer-sized Ag catalyst particles are used,[32] deep, quasi-ordered nanoporous structures are obtained from both orientations with Ag nanoparticles obtained by the use of Tollen's reagent (Fig. 3). The interesting features of this catalyst and process include: (1) the wide range of particle sizes, as the catalyst particles used here varied from 100 nm to 1 μm in size; (2) the nonspherical Ag nanoparticle

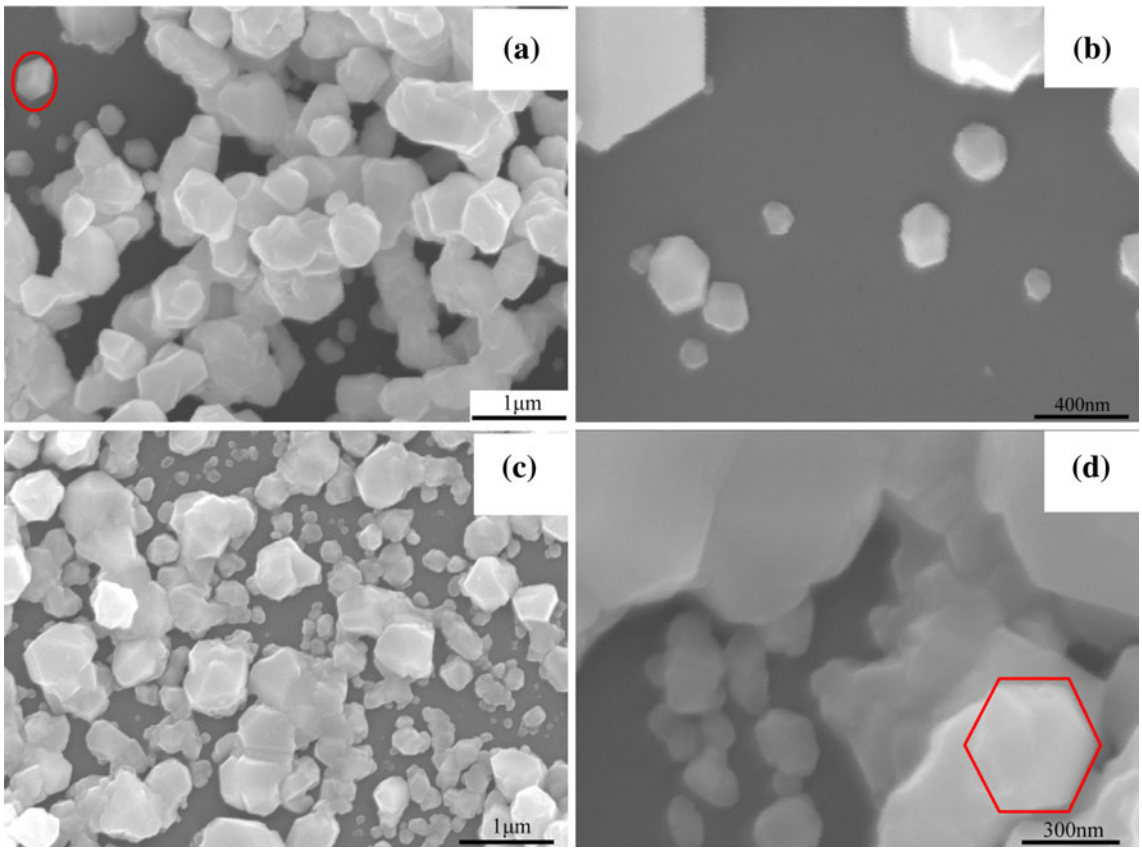

Fig. 1. SEM images of Ag particle deposition by the silver-mirror reaction on (a, b) *p*-Si (100) and (c, d) *p*-Si (111) wafers.

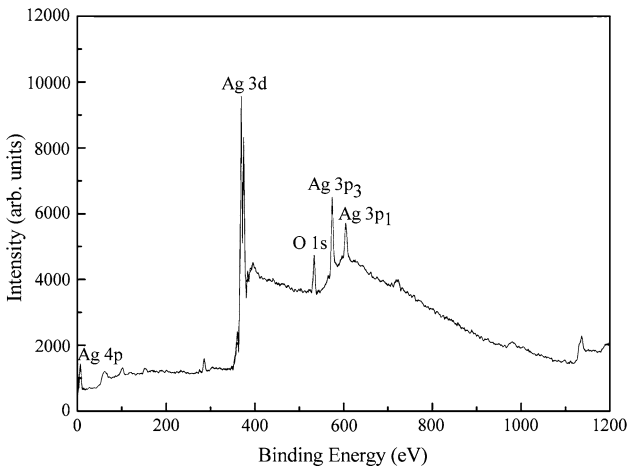

Fig. 2. XPS spectrum of Ag-particle-decorated *p*-Si (100) produced by the silver-mirror reaction.

shapes; (3) the molar ratio of HF:H_2O_2 = 1:2.9, as the composition of the etchant used here lies just inside the range for pore formation and is close to the composition yielding maximum Ag particle penetration rates;[20] and (4) the use of long etch times to allow the etch to proceed under conditions of sparse particle densities which are not present at the beginning of the etch.

Beyond these observations, there are several striking features of the etched Si morphology. First, most of the etched structures display well-defined shapes, with rectangular and hexagonal pores dominating Si (100) and Si (111), respectively. In addition, the internal openings of these structures range from 1 μm to 4 μm, significantly larger than the centroid of the Ag particle distribution. However, there is a striking similarity in pore size among noncoalesced pores, especially for the rectangular pores on Si(100) shown in Fig. 3b. This is surprising in light of the wide dispersion in Ag particle sizes and states of aggregation evident in Fig. 1.

Pore Side-Walls and Sizes

In addition to the gross size and shape distributions, interesting multiscale features are observed in the MacEtch pores. Terraced steps are present on the side-walls of the etched pores formed on both Si (100) and Si (111) substrates in Fig. 3c, d, for example in the areas indicated by the circle in Fig. 3d. The origin of this interesting morphology cannot be definitively assigned at present, however it is consistent with both transverse particle motion, which might be caused by the evolution of H_2, and the nonspherical shapes of the Ag catalyst particles. The Ag-catalyzed MacEtch rate for Si can be as fast

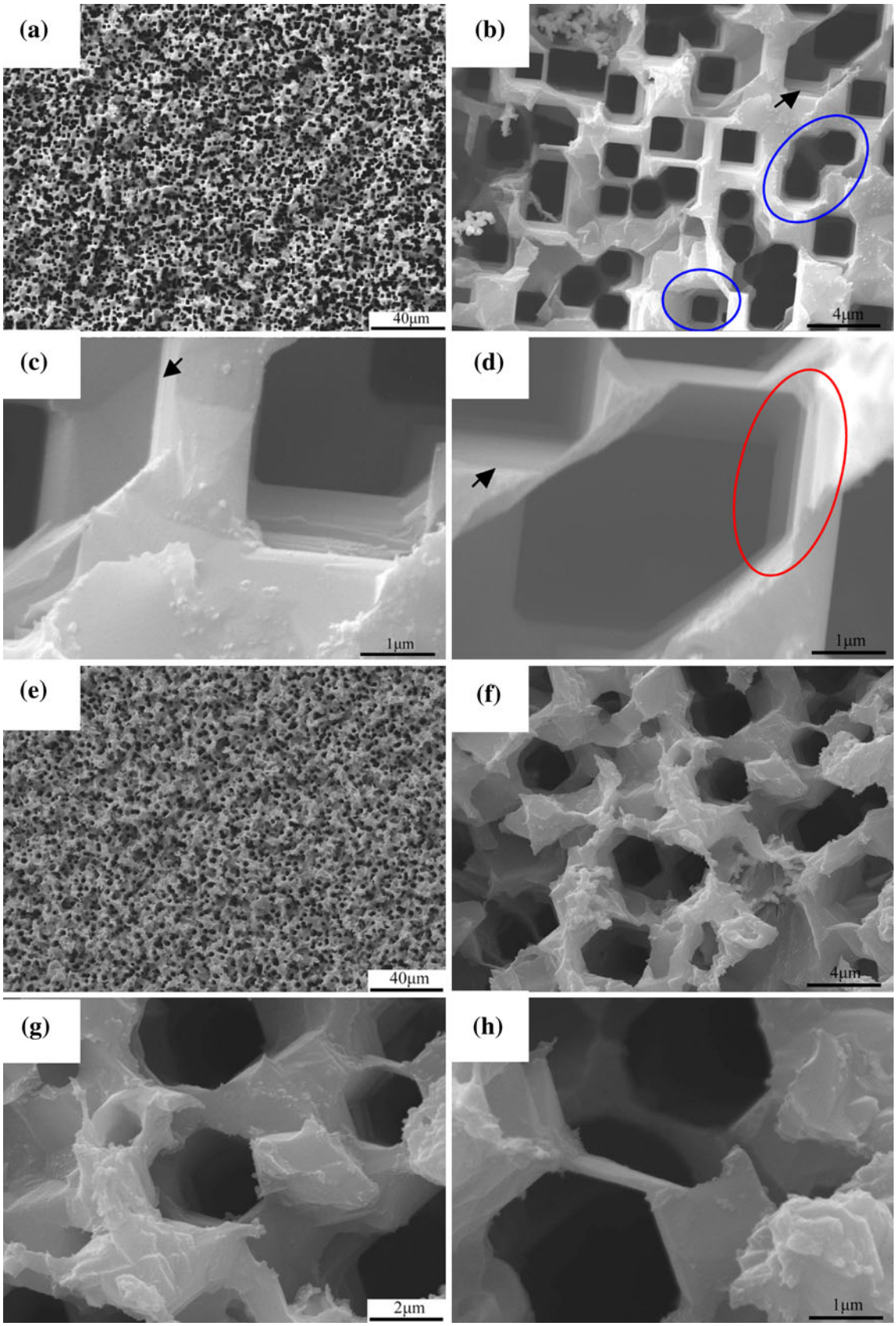

Fig. 3. SEM images of *p*-Si wafers subjected to MacEtch in 1:1:1 (v:v:v) HF (49%):H_2O_2 (30%):ethanol solution for 12 h at 300 K by using catalytic Ag particles deposited on Si via silver-mirror reaction. The top macroporous layers have been removed by dipping in NaOH (1%) for 15 min. The wafers used are *p*-Si (100) for (a–d) and *p*-Si (111) for (e–h). Images are displayed at different magnifications and orientations.

as 1 μm min^{-1},[14] so by reaction (5), the rate of H_2 generation must be correspondingly large, as evidenced by the observation of intense, prolonged bubble evolution. So, it is plausible to assign the large pore sizes and the rough pore side-walls, as evident when checking the cross-section (Fig. S3), to agitation of the Ag nanoparticles caused by evolving H_2 gas. Another striking feature relevant to the convection of Ag nanoparticles is the frequent observation of helical nanopores, such as those shown in the cross-sectional SEM micrographs in Fig. S3. Thus, while the basic pore shape observed in plan view (Fig. 3b, d) is retained except for a small amount of corner rounding, oblique and cross-sectional views lend support to the idea that Ag nanoparticles are strongly convected during the MacEtch process.

Telescoping Pores

Frequently, MacEtch results in formation of conical pores.[32] The analogous behavior observed here is that the size of the internal pore opening diminishes stepwise with depth. This is particularly clear in the highlighted pore at the bottom center of Fig. 3b. The sudden step changes in pore size with depth may result from the production of smaller Ag particles, for example, by disruption of Ag nanoparticle clusters into smaller particles. An alternative explanation could be based on the observation that similar changes occurring during MacEtch of *p*-Si (100) using thermally evaporated silver[22] could be initiated by smaller Ag nanoparticles condensed from Ag^+ dissolved from larger Ag particles.[25] However, there is no direct evidence to confirm extensive dissolution of noble metals in HF/H_2O_2, and Ostwald ripening would be expected to lead to growth of large particles at the expense of small particles.[33,34] Also, if a significant amount of silver existed in the form of Ag^+ ions, in the absence of a more suitable reducing agent, the displacement reaction between Ag^+ and silicon, i.e., Eq. (6), would occur, resulting in isotropic etching, contrary to observation. Thus, it is more likely that H_2 bubble-mediated convection cleaves larger Ag clusters into smaller ones and that these newly formed smaller particles produce vertically organized pores with smaller size at greater depth.

Reflectivity and Surface Energy

One of the goals of this research is to produce materials with enhanced antireflection behavior. Figure 4 shows the reflectivity of samples in the wavelength range of 300 nm $\leq \lambda <$ 800 nm before and after etching. The reflectivity for both orientations of wafers declines after etching, with the change being somewhat larger for *p*-Si (100). The antireflective properties may be further improved by combining MacEtch-produced materials with other strategies to produce antireflection coatings,

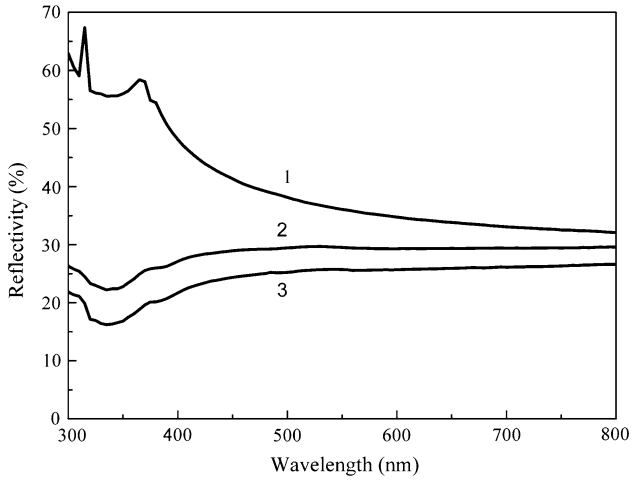

Fig. 4. Reflectivity of samples before and after MacEtch. Curves 1, 2, and 3 represent unetched *p*-Si (100), etched *p*-Si (111), and etched *p*-Si(100) samples, respectively. The processes used to produce samples 2 and 3 are the same as those illustrated in Fig. 3.

e.g., deposition of nanoscale structured SiN_x on textured surfaces[35] and through optimization of the MacEtch process; for example, the reflectance of MacEtch *p*-Si was lowered to $R \approx 10\%$ by greatly reducing the etch time for both kind of wafers, which resulted in quasi-ordered silicon micro/nanostructures being replaced by completely random micro/nanopores mixed with spherical nanoscale features. These latter structures exhibit sufficiently small reflectance, comparable to results obtained using the hot wire method,[36] for potential use as light-trapping layers for silicon solar cells.

CONCLUSIONS

Deposition of catalytic Ag nanoparticles on *p*-Si (100) and (111) wafers by the silver-mirror reaction produces a highly active surface architecture which supports the MacEtch process. Quasi-ordered silicon micro/nanostructures are obtained, and the dramatic differences in morphology between the (100) and (111) surfaces appears to reflect both the underlying crystal orientation as well as complex dynamical processes during etching. These processes reflect the size, shape, and symmetry of the deposited catalyst particles and the rate of evolution of H_2 during etching. The evolution of H_2 throughout the etching processes strongly suggests that the mechanism of etching is governed by separate anodic and cathodic redox processes, i.e., Eqs. (1)–(5), rather than galvanic displacement Eq. (6). The resulting surface reflectivity is reduced relative to the unetched substrates, lying in the range where antireflective properties become technologically interesting. Finally, the stepped side-walls which are characteristic features of these structures might facilitate deposition of noble-metal nanoparticles, which could be used, for example, in high-sensitivity chemical sensing,[13] or as special channels or catalyst

supports for application in embedded microfluidic systems.[37]

ACKNOWLEDGEMENTS

This work was supported by the Program for New Century Excellent Talents in University of China (NCET-06-0337) and by the US National Science Foundation NSF 0807816. The authors gratefully acknowledge B. Duan for valuable discussions.

ELECTRONIC SUPPLEMENTARY MATERIAL

The online version of this article (doi:10.1007/s11664-011-1771-1) contains supplementary material, which is available to authorized users.

REFERENCES

1. M. Spiegel, C. Gerhards, F. Huster, W. Jooss, P. Fath, and E. Bucher, *Sol. Energy Mater. Sol. Cells* 74, 175 (2002).
2. L.A. Dobrzanski and A. Drygala, *J. Mater. Process. Technol.* 191, 228 (2007).
3. Y. Kanamori, M. Sasaki, and K. Hane, *Opt. Lett.* 24, 1422 (1999).
4. W.A. Nositschka, O. Voigt, P. Manshanden, and H. Kurz, *Sol. Energy Mater. Sol. Cells* 80, 227 (2003).
5. Y.F. Huang, Y.J. Jen, K.H. Chen, L.C. Chen, *Nanoengineering: Fabrication, Properties, Optics, and Devices V,* Vol. 7039 (2008).
6. K.S. Lee, M.H. Ha, J.H. Kim, and J.W. Jeong, *Sol. Energy Mater. Sol. Cells* 95, 66 (2011).
7. S. Chattopadhyay and P.W. Bohn, *J. Appl. Phys.* 96, 6888 (2004).
8. S. Chattopadhyay, X.L. Li, and P.W. Bohn, *J. Appl. Phys.* 91, 6134 (2002).
9. X. Li and P.W. Bohn, *Appl. Phys. Lett.* 77, 2572 (2000).
10. X.L. Li, Y.W. Kim, P.W. Bohn, and I. Adesida, *Appl. Phys. Lett.* 80, 980 (2002).
11. M. Matsumura, K. Tsujino, and Y. Nishimoto, *Sol. Energy Mater. Sol. Cells* 90, 100 (2006).
12. S. Koynov, M.S. Brandt, and M. Stutzmann, *Appl. Phys. Lett.* 88, 203107 (2006).
13. B.K. Duan and P.W. Bohn, *Analyst* 135, 902 (2010).
14. W. Chern, K.J. Yu, D. Chanda, J.C. Shin, J.A. Rogers, and X.L. Li, *2010 23rd Annual Meeting of the IEEE Photonics Society*, Vol 718 (2010).
15. J. Zhu, Z.P. Huang, Y. Wu, H. Fang, N. Deng, and T.L. Ren, *Nanotechnology* 17, 1476 (2006).
16. J. Zhu, K.Q. Peng, and Z.P. Huang, *Adv. Mater.* 16, 73 (2004).
17. N. Fang, W. Chern, K. Hsu, I.S. Chun, B.P. de Azeredo, N. Ahmed, K.H. Kim, J.M. Zuo, P. Ferreira, and X.L. Li, *Nano Lett.* 10, 1582 (2010).
18. C.P. Wong, O.J. Hildreth, and W. Lin, *ACS Nano* 3, 4033 (2009).
19. K. Rykaczewski, O.J. Hildreth, C.P. Wong, A.G. Fedorov, and J.H.J. Scott, *Adv. Mater.* 23, 659 (2011).
20. S. Bastide, C. Chartier, and C. Levy-Clement, *Electrochim. Acta* 53, 5509 (2008).
21. J. Zhu, H. Fang, X.D. Li, S. Song, and Y. Xu, *Nanotechnology* 19, 255703 (2008).
22. J. Zhu, H. Fang, Y. Wu, and J.H. Zhao, *Nanotechnology* 17, 3768 (2006).
23. Z.P. Huang, T. Shimizu, S. Senz, Z. Zhang, X.X. Zhang, W. Lee, N. Geyer, and U. Gosele, *Nano Lett.* 9, 2519 (2009).
24. K. Nishioka, T. Sueto, and N. Saito, *Appl. Surf. Sci.* 255, 9504 (2009).
25. S. Yae, H. Tanaka, T. Kobayashi, N. Fukumuro, and H. Matsuda, *Phys. Status Solidi C: Conf. Crit. Rev.* 2, 3476 (2005).
26. K.Q. Peng, H. Fang, J.J. Hu, Y. Wu, J. Zhu, Y.J. Yan, and S. Lee, *Chem. Eur. J.* 12, 7942 (2006).
27. F.M. Liu and M. Green, *J. Mater. Chem.* 14, 1526 (2004).
28. K.Q. Peng, A.J. Lu, R.Q. Zhang, and S.T. Lee, *Adv. Funct. Mater.* 18, 3026 (2008).
29. S. Siggia and E. Segal, *Anal. Chem.* 25, 640 (1953).
30. J.G. Allpress and J.V. Sanders, *Surf. Sci.* 7, 1 (1967).
31. C.M. Wang, W.C. Ye, C.M. Shen, J.F. Tian, C. Hui, and H.J. Gao, *Solid State Sci.* 11, 1088 (2009).
32. M. Matsumura, C.L. Lee, K. Tsujino, Y. Kanda, and S. Ikeda, *J. Mater. Chem.* 18, 1015 (2008).
33. Lasaga AC (ed) Kinetic Theory in the Earth Sciences. (Princeton University Press, NJ, Princeton, 1998).
34. T. Hadjersi, N. Megouda, G. Piret, R. Boukherroub, and O. Elkechai, *Appl. Surf. Sci.* 255, 6210 (2009).
35. K.C. Sahoo, Y.M. Li, and E.Y. Chang, *IEEE Trans. Electron Dev.* 57, 2427 (2010).
36. T. Sato, T. Sugiura, M. Ohtsubo, S. Matsuno, and M. Konagai, *Jpn. J. Appl. Phys. Part 1* 46, 6796 (2007).
37. D.P. Kim, Z.Y. Xiao, Y. Zhao, A.J. Wang, and J. Perumal, *Lab Chip* 11, 57 (2011).